LEVEL III

ADE 000 304 (12)

NRL Memorandum Report 3930

B.S

Numerical Simulation of Collapsing Turbulent Wakes

Comparison of Turbulence and Closures and Numerical Schemes

A. WARN-VARNAS, S. A. PIACSEK, G. HAIN, AND J. BLOCK

Plasma Physics Division

March 22, 1979

79 04 30 006

NAVAL RESEARCH LABORATORY
Washington, D.C.

UNCLASSIFIED

SECURITY CLASSIFICATION OF THIS PAGE (When Data Entered)

REPORT DOCUMENTATION PAGE		READ INSTRUCTIONS BEFORE COMPLETING FORM
1. REPORT NUMBER NRL Memorandum Report 3930	2. GOVT ACCESSION NO.	3. RECIPIENT'S CATALOG NUMBER
4. TITLE (and Subtitle) NUMERICAL SIMULATION OF COLLAPSING TURBULENT WAKES — Comparison of Turbulence Closures and Numerical Schemes		5. TYPE OF REPORT & PERIOD COVERED Interim report on a continuing NRL problem. 6. PERFORMING ORG. REPORT NUMBER
7. AUTHOR(s) A. Warn-Varnas*, S. A. Piacsek*, G. Hain and J. Block		8. CONTRACT OR GRANT NUMBER(s) ARPA Order 2152
9. PERFORMING ORGANIZATION NAME AND ADDRESS Naval Research Laboratory Washington, D.C. 20375		10. PROGRAM ELEMENT, PROJECT, TASK AREA & WORK UNIT NUMBERS NRL Problem G01-11
11. CONTROLLING OFFICE NAME AND ADDRESS Advanced Research Projects Agency 1400 Wilson Boulevard Arlington, Virginia 22209		12. REPORT DATE March 22, 1979 13. NUMBER OF PAGES 35
14. MONITORING AGENCY NAME & ADDRESS(if different from Controlling Office)		15. SECURITY CLASS. (of this report) UNCLASSIFIED 15a. DECLASSIFICATION/DOWNGRADING SCHEDULE

16. DISTRIBUTION STATEMENT (of this Report)

Approved for public release; distribution unlimited.

17. DISTRIBUTION STATEMENT (of the abstract entered in Block 20, if different from Report)

18. SUPPLEMENTARY NOTES

*Permanent address: NORDA, NSTL Station, Mississippi 39529
Report actually written November 1977.

19. KEY WORDS (Continue on reverse side if necessary and identify by block number)

Turbulent wakes
Numerical simulation

20. ABSTRACT (Continue on reverse side if necessary and identify by block number)

The collapse of a partially mixed region generated by a prescribed amount of turbulence deposited on a linearly stratified ambient ocean is studied numerically. Different turbulent closures such as first and second order are used to model the turbulent stresses. The resulting equations are solved numerically in a finite-difference formalism of the primitive form of the equations in a box region several times the size of the mixed region. The resulting maximum observed mean field velocities, densities, and turbulent energies in the fluid are obtained and cross-compared for different closures and numerical methods.

DD FORM 1 JAN 73 1473 EDITION OF 1 NOV 65 IS OBSOLETE
S/N 0102-014-6601

UNCLASSIFIED

SECURITY CLASSIFICATION OF THIS PAGE (When Data Entered)

79 04 06 006

CONTENTS

I. INTRODUCTION

This work was undertaken with the objective of benchmarking various turbulence codes against each other, and to study their sensitivity to resolution and numerical techniques. The benchmarking process usually involves comparison of numerical simulation results obtained for the same physical experiment but employing different numerical methods and turbulence closure approximations.

In this study the benchmarking and sensitivity tests were performed on a test case devised by Lewellen (1974), which consists of the collapse of a turbulent mixed region in a stratified fluid. We shall refer to this case hereafter as the LT case. In particular, the results of four numerical experiments will be presented: (a) a study of the effect of mesh size and stretching on the collapse process and internal wave propagation; (b) depth dependence resulting from the presence of the free top boundary; (c) comparison of Launder's (1975) second order closure scheme with its contracted first order version; and (d) comparison of Lewellen's numerics with ours on his test problem.

The aim of experiment (a) was to find the minimum resolution necessary to simulate correctly the hydrodynamic processes near the collapse region, and the internal waves propagating between this region and the surface. This helped to determine the smallest amount of computer time and storage that one could "get away with" in running production jobs.

Experiment (b) was designed to study the effect on the maximum velocities of the presence of a free surface, serving as a reflector of internal waves.

The aim of experiment (c) was to establish the difference in the generated internal wave field when collapse is modeled by first- and second-order closure turbulence models, respectively. It also tried to ascertain whether first-order models, which require much less computer time and storage, would in fact suffice for the problems of interest.

Experiment (d), tried to determine whether differences resulting from the employment of various numerical schemes would in fact be comparable to differences resulting from turbulence models, resolution changes or depth dependence.

II. MODEL DESCRIPTION

The inviscid fluid code used in experiment (b) is identical to the mean field part of the turbulence code used in the other experiments, with the Reynolds's stresses set equal to zero. These equations, together with the corresponding numerical schemes, have been

Note: Manuscript submitted December 11, 1978.

presented in a paper by Dugan and Warn-Varnas (1974) and will not be discussed separately here.

Our second-order closure approximations for turbulence modeling follow the Launder (1974) philosophy. The main difference between this scheme and that presented by Lewellen (1974) is in the closing of the triple velocity correlations, and the correlations between the pressure and the velocity gradients or the velocities.

We shall now proceed to describe the Launder turbulence model. We partition all dependent variables into their mean and fluctuating parts, e. g. $u_i = \bar{u}_i + u_i'$, and write transport equations for the time evolution of the mean fields and the second-order correlations, e. g. $u_i'u_j'$:

$$\frac{D\bar{u}_i}{Dt} = -\frac{1}{\rho_o}\frac{\partial \bar{p}}{\partial x_i} + \frac{\rho}{\rho_o} g_i - \frac{\partial}{\partial x_j}\overline{(u_i'u_j')} + \nu\nabla^2\bar{u}_i \tag{1}$$

$$\frac{D\bar{\rho}}{Dt} = -\frac{\partial}{\partial x_j}\overline{(u_j'\rho')} + \kappa\nabla^2\bar{\rho} \tag{2}$$

$$\frac{\partial \bar{u}_i}{\partial x_i} = 0 \tag{3}$$

$$\frac{D}{Dt}\overline{(u_i'u_j')} = -\left\{\overline{u_i'u_k'}\frac{\partial \bar{u}_j}{\partial x_k} + \overline{u_j'u_k'}\frac{\partial \bar{u}_i}{\partial x_k}\right\} + \frac{1}{\rho_o}\left\{\overline{u_i'\rho'}\,g_j + \overline{u_j'\rho'}\,g_i\right\}$$

$$-2\nu\overline{\left(\frac{\partial u_i'}{\partial x_k}\frac{\partial u_j'}{\partial x_k}\right)} + \overline{\frac{p'}{\rho_o}\left(\frac{\partial u_i'}{\partial x_j} + \frac{\partial u_j'}{\partial x_i}\right)} \tag{4}$$

$$-\frac{\partial}{\partial x_k}\left\{\overline{u_i'u_j'u_k'} + \frac{1}{\rho_o}\left(\delta_{ik}\overline{u_j'p'} + \delta_{jk}\overline{u_i'p'}\right)\right\}$$

$$\frac{D}{Dt}\overline{(u_i'\rho')} = -\overline{u_i'u_k'}\frac{\partial \bar{\rho}}{\partial x_k} - \overline{u_k'\rho'}\frac{\partial \bar{u}_i}{\partial x_k} + \frac{g_i}{\rho_o}\overline{\rho'^2}$$

$$-(\kappa + \nu) \overline{\frac{\partial \rho'}{\partial x_k} \frac{\partial u_i'}{\partial x_k}} + \overline{\frac{p'}{\rho_o} \frac{\partial \rho'}{\partial x_i}} - \frac{\partial}{\partial x_k} \left(\overline{u_i' u_k' \rho' + \frac{p' \rho'}{\rho_o}} \right) \tag{5}$$

The following closure approximations are introduced by Launder (1975):

[C1] Pressure-strain correlation:

$$\overline{\frac{p'}{\rho_o} \left(\frac{\partial u_i'}{\partial x_j} \frac{\partial u_j'}{\partial x_j} \right)} = -c_1 \frac{\varepsilon}{K} \left(\overline{u_i' u_j'} - \frac{2}{3} \delta_{ij} K \right) - c_2 \left(P_{ij} - \frac{2}{3} \delta_{ij} P \right) \tag{6}$$

where

$$K = \frac{1}{2} \overline{u_i' u_i'} \ , \ 3 \nu \overline{\frac{\partial u_i}{\partial x_k} \frac{\partial u_i}{\partial x_k}} = \delta_{ij} \varepsilon \tag{7a, b}$$

$$P_{ij} = \left(\overline{u_i' u_k'} \frac{\partial \bar{u}_j}{\partial x_k} + \overline{u_j' u_k'} \frac{\partial \bar{u}_i}{\partial x_k} \right) + \frac{1}{\rho_o} \left(\overline{\rho' u_i'} g_j + \overline{\rho' u_j'} g_i \right) \tag{7c}$$

$$P = - \left(\overline{u_i' u_k'} \frac{\partial \bar{u}_i}{\partial x_k} - \frac{g_i}{\rho_o} \overline{u_i' \rho'} \right) \tag{8}$$

and

$$c_1 = 3.0, \ c_2 = .4 \tag{8a}$$

[C2] Triple velocity correlation:

$$\overline{u_i'u_j'u_k'} = - c_3\frac{K}{\varepsilon}\overline{u_i'u_k'}\frac{\partial}{\partial x_k}(\overline{u_i'u_j'}),\ c_3 = .22 \tag{9}$$

[C3] Pressure-density gradient correlation

$$\overline{\frac{p'}{\rho_o}\frac{\partial \rho'}{\partial x_i}} = - c_{1t}\ \frac{\varepsilon}{k}\overline{u_i'\rho'} - c_{2t}P_{it} \tag{10}$$

where

$$c_{1t} = 3.2 \text{ and } c_{2t} = .5$$

and

$$P_{it} = -\left(\overline{u_k'\rho'}\ \frac{\partial \bar{u}_i}{\partial x_k} - \frac{g_i}{\rho_o}\ \overline{\rho'^2}\right) \tag{11}$$

[C4] Double velocity-density correlation

$$\overline{u_k'u_i'\rho'} = - c_{3t}\ \frac{K}{\varepsilon}\ \overline{u_k'u_\ell'}\ \frac{\partial}{\partial x_\ell}\ (\overline{u_i'\rho'}),\ c_{3t} = .22 \tag{12}$$

with the quantity

$$\frac{\partial}{\partial x_k}\left(\delta_{ik}\ \frac{\overline{u_j'p'}}{\rho_o} + \delta_{jk}\ \frac{\overline{u_i'p'}}{\rho_o}\right) \tag{13}$$

set equal to zero. The neglect of pressure diffusion has some experimental justification, with the most persuasive being that of Irwin (1974).

The length scale of the energy containing eddies is obtained from a relation between the turbulence energy density K and the dissipation function ϵ:

$$\ell = \frac{K^{3/2}}{\epsilon} . \tag{14}$$

Lewellen (1974) makes a somewhat different closure approximation for the correlations [C1] - [C4], using the relation (14). For the pressure-strain correlation [C1] he sets $c_2 = 0$ in (6), which essentially omits terms that represent the effects of gravity and production of turbulence by the mean velocity shear. A similar effect is achieved by setting $c_{2t} = 0$ in (10) for the pressure-density gradient correlation [C3]. In the correlations [C2] and [C4] Lewellen neglects the terms involving $\overline{u_i' u_k'}$, where $i \neq k$, and for the remaining term $\frac{K}{\epsilon} \overline{u_k' u_k'}$ he substitutes from (7a) and (14). Thus, [C2] becomes

$$\overline{u_i' u_j' u_k'} = - 2\, c_3\, \ell K^{1/2} \frac{\partial}{\partial x_k} (\overline{u_i' u_j'}) , \tag{15}$$

and [C4]

$$\overline{u_i' u_j' \rho'} = - 2\, c_{3t}\, \ell K^{1/2} \frac{\partial}{\partial x_j} (\overline{u_i' \rho'}) . \tag{16}$$

To obtain a first-order closure scheme, we will make the following closures of the second-order correlations:

$$\overline{u_i' u_j'} = - c_u \frac{K^2}{\epsilon} \left(\frac{\partial \bar{u}_i}{\partial x_j} + \frac{\partial \bar{u}_j}{\partial x_i} \right) \tag{17}$$

$$\overline{u_i' \rho'} = - \frac{c_u}{\sigma_o} \frac{K^2}{\epsilon} \frac{\partial \bar{\rho}}{\partial x_i} ; \quad c_u = .09 \text{ and } \sigma_o = 1.0 \tag{18}$$

The predictions of $\overline{u_i'^2}$ proceeds in the same way as in the second-order theory.

III. RESULTS AND DISCUSSION

A. Mesh-size Dependence of Maximum Velocities

The second-order closure model of Launder (1975) described above was used to study the sensitivity to resolution of the wake region. In order to save computer time, initial conditions somewhat different from Lewellen (1974) were employed.

The computational region consisted of a square of 200 cm by 200 cm, with the radius of the mixed region being a = 15 cm. A linear stratification of N = .707 sec^{-1} was specified everywhere in the fluid at t = 0, and an initial patch of turbulence energy was deposited according to the distribution law

$$\overline{u'^2} = \overline{w'^2} = \frac{1}{2} A_T e^{-r^4/a^4}, \tag{19}$$

where $A = 10^3 cm^2/sec^2$ and a is the radius. The mean velocities and all second-order correlations were set to zero at t = 0.

Figures 2 and 3 show the comparison of the maximum horizontal and vertical velocities obtained with resolutions of 5, 7, and 9 grid points in the (initial) wake radius. We observe an approach to asymptotic stabilization of the results for 7 or more mesh points. The percentage deviation of the 5 grid point results from the asymptotic results is 8% for both u_{max} and w_{max}.

B. Depth Dependence of Maximum Velocities

This experiment was carried out by the inviscid code reported on by Dugan and Warn-Varnas (1974) in NRL Memo Report #2597. The resolution of the wake was 8 grid points in the vertical and 7 in the horizontal in all cases. Figures 4 and 5 show the results for depth-to radius ratios of 2 and 8, respectively; the percentage variation in the maximum velocities is about 8%. These values occurred near the edge of the wake, and can be associated with the circulation that takes place during the primary collapse phase of the wake.

It was also important to determine whether the results would change further if the depth-to-radius ratio of 8 is increased. To simulate the asymptotic case of an infinite ratio, an absorbing liner was placed outside the wake; mathematically this is represented by a region

of high Newtonian viscosity. The following expression, suggested by Roberts (1972), was used:

$$\frac{du}{dt} = -.5 \exp\left\{ \mathrm{SINH}\left[\mathrm{SINH}\,(-x/.125\,L_x)\right] + \mathrm{SINH}\left[\mathrm{SINH}\,(-z/.125\,L_z)\right]\right\} \quad (20)$$

where L_x and L_z are the dimensions of the computational domain in the x and z regions, respectively. The results were found to be equivalent to those of the ratio of 8.

C. Comparison of 1st and 2nd - Order Closure Results

These experiments were performed with the Launder (1975) turbulence model described in Section II above. The test case on which they were compared was devised by Lewellen (1974), and is referred to in this paper as the LT case. The computational domain was a square region of area $10^4 \times 10^4\ cm^2$. Because of the inherent symmetry of the problem in both x and z in the case of a linear ambient density stratification, only a quarter of the whole region needs to be simulated. The "radius" a of the turbulent region, i.e. the half-width of a gaussian distribution of perturbation density, was 500 cm, making the depth-to-radius ratio of this problem 20. A scaling analysis of Eqs. (1) - (18) was performed using a length scale a, a velocity scale u and a density variation scale a $\frac{\partial \rho_o}{\partial z}$. Here u is the free stream velocity of a self-propelled object that in fact never appears explicitly in the model, using a time scale $t_o = a/u$ the following nondimensional parameters emerge:

$$N^2 = -\frac{g}{\rho_o}\frac{\partial \rho_o}{\partial t} = \text{constant}, \quad (21a)$$

$$Fr = \frac{u}{aN}, \quad (21b)$$

$$Ri = \frac{1}{Fr^2 K'_{max}}. \quad (21c)$$

Here K'_{max} is the maximum value of the initial nondimensionalized turbulence energy density, N is the Brunt-Vaisala frequency, Fr is the Froude number and Ri is a Richardson number based on both the stream velocity and the turbulence velocity. In nondimensional form, the initial conditions become

$$\delta = z \qquad z \le 1$$

$$\delta = z e^{-2(r^2 - 1)} \qquad z > 1 \quad (22)$$

$$K = \frac{1}{4}(.0108)\, e^{-1.38 r^2}, \quad r^2 = x^2 + z^2, \quad (23)$$

for the perturbation density and the turbulence energy, respectively.

To start a specific calculation, we have to specify Fr and Ri, or Fr and K'_{max}. In the experiments performed Ri = .872 and Fr = 10.3. All correlations of form $\overline{u_i'\rho'}$ and $\overline{u_i'u_j'}$ with $i \neq j$ were set zero at t = 0. Finally, one has to specify the integral length scale of turbulence ℓ introduced in (14), and also referred to as the macroscale. It is determined by relating it to a fraction of the distance from the center of the wake to where the turbulence drops to a quarter of its maximum strength. In practice, one finds both the length scales ℓ_x and ℓ_z that measure the distance from the axis to the isoline $K = .25\, K_{max}$ of turbulence along the x and z directions, respectively, and then obtains ℓ according to the formula

$$\ell = \frac{.2\ \ell_x^2 \ell_z}{\ell_x^2 + \ell_z^2}. \tag{24}$$

Figures 7 and 8 show the first and second order closure results for u_{max}, w_{max}, $\hat{\rho}_{max}$ and q_{max}, where $q_{max} = (2\, K_{max})^{1/2}$ is the turbulence velocity. The location of the maxima of the velocities in time are approximately the same, but the second order magnitudes are somewhat higher. The second order density perturbation is also higher, whereas the turbulence velocity is slightly lower. Table I gives the exact numbers at $t \simeq .35$ nondimensional time. Figure 9 illustrates the time development of the various forms of energy in time. Both the kinetic and available potential energy associated with second order closure exceed the first order values by almost a factor of 2. The turbulence energy curve is the same for both closures, indicating a possible dominance of the decay term in the turbulence energy equation. The available potential energy is defined as

$$APE = \frac{1}{2} \int dv (\bar{\rho} - \bar{\rho}_I)^2 \left(\frac{d\rho_I}{dz}\right)^{-1}, \tag{25}$$

where $\bar{\rho}_I$ is the initial mean density, and the deviation from $\bar{\rho}_I$ represents the largest fraction of energy in each model. A possible explanation for the potential energy behavior is given further below, in connection with an analysis of the magnitude of terms in the density Eq. (2).

Next we proceed to a comparison of the 1^{st} and 2^{nd}-order results for the temperature-velocity correlations and the off-diagonal Reynold's stresses. Figure 10 exhibits the turbulent transport of density fluctuations $\overline{w'\rho'}$ as a function of z at x/a = .57 and at $t' = Nt/2\pi = .37$. Differences in both magnitude and shape are observable, with the second order transport everywhere negative and the first-order reversing sign half-way to the vanishing point.

Since in 1^{st}-order theory $\overline{w'\rho'} = -K \frac{\partial \bar{\rho}}{\partial z}$, the turbulent transport follows the sign of $\frac{\partial \bar{\rho}}{\partial z}$ so that outside the wake, up to $r \lesssim 2a$, there is a counter-gradient density flux according to 2^{nd}-order theory. This would imply that negative entrainment is being generated by the first-order model, i.e. some kind of free-convective turbulence that produces mean potential energy.

Figure 11 displays the Reynold's stress $\overline{u'w'}$ at $x/a = .57$, $t' = 37$. In this case there are noteworthy differences in the magnitude, shape and sign of the stresses, with the second-order stress being everywhere negative and the first-order positive out to about 1.3 radius. However, since the effective viscous dissipation is given by $\frac{\partial}{\partial z} (\overline{u'w'})$ it is the slopes of the two curves that should be compared. They both exhibit a negative slope out to about $z \gtrsim a$, i.e. the edge of the (original) wake, indicating normal viscous dissipation. Then for $a \lesssim z \lesssim 1.5\,a$ in both cases the slopes become negative, indicating a possible mean flow enhancement by the eddies. The big discrepancy occurs in the magnitude of the dissipation, with the first-order results exceeding the second-order values by a factor of ten. In the case of the buoyancy flux ratio in Figure 10 this ratio is only ~ 3.

Next we investigated the magnitude of the individual terms in the mean density transport Eqs. (1). The results are summarized in Figure 12, showing each term as a function of horizontal distance at a height $z/a = .587$ above the center of the wake, at time $t' = Nt/2\pi = .37$. It is evident that transport by the 'thermal stresses' or 'buoyancy fluxes $\overline{u'\rho'}$ and $\overline{w'\rho'}$ is comparable to that by the mean flow in the first-order results. On the other hand, in the second-order results the turbulent contributions are two orders of magnitude less than the mean advection terms. This great discrepancy between first- and second-order closure simulation explains the difference by a factor of two in the available potential energy.

D. Evaluation of Lewellen and Warn-Varnas Numerics on the LT Benchmark Case

It was of interest to know how the present code would perform on the LT Benchmark case if we set the turbulence closure and pertinent constants identical to Lewellen's, effectively comparing the different numerics. To this end we have set the closure constants $c_{2t} = c_2 = 0$ in equations (1) - (12), leading to an exclusion of gravitational contributions to the pressure-strain correlation. The other constants have also been made to agree with Lewellen's values. Using equation (14) relating the turbulence length scale, dissipation

function and turbulence intensity, the pressure-strain correlation (6) becomes

$$\overline{\left(\frac{p'}{\rho_o}\frac{\partial u_i'}{\partial x_j}+\frac{\partial u_j'}{\partial x_i}\right)} = -\frac{q}{\ell}\left(\overline{u_i'u_j'}-\frac{\delta_{ij}}{3}q^2\right) \tag{26}$$

where $q = \sqrt{2K} = \sqrt{\overline{u_i'u_i'}}$. In a anologous way $\overline{\frac{p'}{\rho_o}\frac{\partial \rho'}{\partial x_i}} = -.75\,\frac{q}{\ell}\,\overline{u_i'\rho'}$

The diffusion term in (4) involving the triple correlation in the reduced form given by (15) simplifies to $\frac{\partial}{\partial x_k}\left[.39\, q\ell \frac{\partial}{\partial x_k}\right]\phi$, with ϕ being the stress calculated and c_3 set to .28. The dissipation correlation for Lewellen's case was closed as

$$2\nu\,\overline{\frac{\partial u_i'}{\partial x_k}\frac{\partial u_j'}{\partial x_k}} = \frac{2bq}{\ell}\overline{u_i'u_j'} - \frac{2a\nu}{\ell^2}\overline{u_i'u_j'}$$

with a = 2.5 and b = .125.

The calculation was performed on a region 20a by 15a (a being the wake radius), with a 40 x 40 grid resolution and placing 8 points of a stretched mesh inside the wake. The results are summarized in Figure 16 and Table I (4th line). The differences in the maximum horizontal and vertical velocities are 8% and 18%, respectively. There is also a shift in the occurrence times, from t' = $Nt/2\pi$ of .35 and .21 to .37 and .24, respectively, with Lewellen's code giving the later values.

Comparing Figure 16 to Figure 6, the most striking difference is the slower decay of the turbulence intensity q for the Lewellen numerics (Figure 6). The most logical source of this discrepancy would be a difference in the constants occurring in the diffusion and decay terms discussed above. The description of the macroscale ℓ would also influence the decay. The differences in the q-decay would also influence the behavior of the maximum horizontal and vertical velocities.

IV. CONCLUSION

Comparison calculations have been made on the collapse motions and internal waves generated by turbulent wakes deposited in a stratified fluid. The main results of the calculations can be summarized as follows:

1. Seven mesh points in a wake radius are sufficient to resolve the collapse process, with five points giving an 8% error in the maximum velocities generated.
2. A change in the depth-to-radius ratio of two-to-eight results in an 8% variation in the maximum velocities. Any further increase in the ratio results in no further velocity variations. These results imply that the presence of the top surface (a density discontinuity) has no great influence on the collapse process, provided the maximum extent of a turbulent wake is less than half its depth.
3. A comparison of 1st and 2nd order turbulence closure schemes showed a 33% variation in the maximum horizontal velocities and a 25% variation in the vertical component, indicating a need for a better tuned or physically correct 1st-order model. Furthermore, a comparison of the correlations $\overline{w'T'}$ and $\overline{u'w'}$ with the second-order results gives evidence of negative density entrainment (free-convective energy release) and mean flow enhancement by the Reynolds stress, respectively, features that 1st-order theory can not reproduce. However, we have not determined the total region size of the fluid where such processes take place, nor their total quantitative contribution to the collapse.
4. Comparison of numerics by Warn-Varnas and Lewellen show a discrepancy of 20%, which made the comparison of the Launder closure with the Lewellen turbulence closure difficult to interpret.

Table I

Comparison of maximum mean velocities for the LT case using different closure schemes and numerics. The horizontal velocity u_{max} and w_{max} are given in dimensionless units, and their respective deviations from the LT results in %.

	U_{max}	W_{max}	δU(%)	δW(%)
LT (Lewellen, 1974)	.0310	.0285	0	0
1st order closure	.0260	.0210	-16	-26
2nd order Launder closure	.0370	.0280	19	-2
2nd order Lewellen closure	.0285	.0235	-8	-18

APPENDIX A

FINITE-DIFFERENCE SCHEME

We shall first discuss the stretching of the mesh and the spatial differencing, then the time differencing and the method used to find the pressure. The stretching of the mesh was accomplished by the use of the function $\xi = (e^{x/x_\ell} - 1)/(e^{x/x_\ell} + 1)$ where x_ℓ is a normalization constant that controls the stretching in the ℓ-th boundary layer. For equal increments $\Delta\xi$ of the function $\xi_i = i\Delta\xi$, a set of coordinate values x_i will be generated such that $\Delta x = x_i - x_{i-1}$ constitute the variable mesh spacings. A similar transformation is effected between η and z. It must be pointed out that the equations are not transformed to a new coordinate system ξ and η, but are directly differenced on the new grids x_i and z_k; the functions ξ and η merely serve the purpose of creating a smoothly varying x and z mesh.

The differencing of the advection terms will be illustrated on the transport part of the horizontal velocity equation. The scheme was presented for constant grids by Piacsek & Williams (1970). We shall denote the coordinate axes by x_i and z_k, the time by $t^n = n\Delta t$, and the value of a dependent variable ϕ as $\phi(x_i, z_k; t^n) = \phi^n_{i,k}$ with the superscript denoting a time level and the subscripts a mesh point location in space. Reference should be made to Figure 1 for inspecting the arrangement of the dependent variable on the various subsets of the staggered mesh. (Note that upper case symbols are used to denote the variables in the figure.) Using these symbols, we have,

$$\frac{1}{4\Delta x_{i+\frac{1}{2}}}\left[(\bar{u}_{i+1} + \bar{u}_i)\bar{u}_{i+1} - (\bar{u}_i + \bar{u}_{i-1})\bar{u}_{i-1}\right]_k +$$

$$+ \frac{1}{4\Delta z_{k+\frac{1}{2}}}\left[(\bar{w}_{i+\frac{1}{2}} + \bar{w}_{i-\frac{1}{2}})_{k+\frac{1}{2}}\,\bar{u}_{i,k+1} - (\bar{w}_{i+\frac{1}{2}} + \bar{w}_{i-\frac{1}{2}})_{k-\frac{1}{2}}\,\bar{u}_{i,k-1}\right].$$

The advantage of this scheme is that it conserves $\bar{u}$ exactly,

$$\sum_{i,k} \bar{u}_{i,k}\frac{\partial \bar{u}_{i,k}}{\partial t}\Delta x_i \Delta z_k = 0$$

when summed over the interior grid points, regardless of whether or not the divergence is zero. For a discussion of this point and the method of evaluating conservation properties the reader is referred to Williams (1969) and Piacsek and Williams (1970). It is known that the boundedness of $\bar{u}^2$ ensures stability and that of $\bar{u}$ does not; furthermore, nonzero divergence is always present when iterative methods are used to find the pressure. The remaining terms in the horizontal velocity equation are differenced as follows:

the pressure term,

$$\frac{1}{\rho}\,\frac{1}{\Delta x_{i+\frac{1}{2}}}\left(\bar{P}_{i+\frac{1}{2}} - \bar{P}_{i-\frac{1}{2}}\right)^n_k ;$$

the Reynolds stress term,

$$-\frac{1}{\Delta x_{i+\frac{1}{2}}}\left[(\overline{u'u'})_{i+\frac{1}{2}} - (\overline{u'u'})_{i-\frac{1}{2}}\right]^n_k - \frac{1}{4\Delta_{zk+\frac{1}{2}}}\left[(\overline{u'u'})_{i+\frac{1}{2},k+\frac{1}{2}}\right.$$

$$\left. + (\overline{u'w'})_{i-\frac{1}{2},k+\frac{1}{2}} - (\overline{u'w'})_{i+\frac{1}{2},k-\frac{1}{2}} - (\overline{u'w'})_{i-\frac{1}{2},k-\frac{1}{2}}\right]^n ;$$

the viscous term,

$$\nu\left\{\frac{1}{\Delta x_{i+\frac{1}{2}}}\left[\frac{1}{\Delta x_{i+1}}(\bar{u}^n_{i+1,k} - \bar{u}^{n+1}_{i,k}) - \frac{1}{\Delta x_i}(\bar{u}^n_{i,k} - \bar{u}^{n-1}_{i-1,k})\right]\right.$$

$$\left. + \frac{1}{\Delta z_{k+\frac{1}{2}}}\left[\frac{1}{\Delta z_{k+1}}(\bar{u}^n_{i,k+1} - \bar{u}^{n+1}_{i,k}) - \frac{1}{\Delta z_k}(\bar{u}^n_{i,k} - \bar{u}^{n-1}_{i,k-1})\right]\right\}$$

The finite-differencing of the forecast equations for the Reynolds and thermal stresses is illustrated on the sample equation,

$$\frac{\partial}{\partial t}\overline{u'u'} = \frac{\partial}{\partial x}\left[\phi\frac{\partial}{\partial x}\overline{u'u'}\right] + \frac{\partial}{\partial z}\left[\phi\frac{\partial}{\partial z}\overline{u'u'}\right]$$

$$- F\,\overline{u'u'} + R$$

in finite-difference form this equation becomes:

$$\frac{\overline{u'u'}^{n+1} - \overline{u'u'}^{n-1}}{2\Delta t} = \frac{1}{\Delta x_{i+\frac{1}{2}}}\left\{\frac{\phi^n_{i+\frac{1}{2}}}{\Delta x_{i+1}}\left[(\overline{u'u'})^n_{i+1} - (\overline{u'u'})^{n+1}_i\right]_k\right.$$

$$
- \frac{\phi^{n}_{i-\frac{1}{2}}}{\Delta x_i}\left[\overline{(u'u')}^{\,n-1}_{i} - \overline{(u'u')}^{\,n}_{i-1}\right]_k \Bigg\} + \frac{1}{\Delta z_{k+\frac{1}{2}}}\Bigg\{ \frac{\phi^{n}_{k+\frac{1}{2}}}{\Delta z_{k+1}}\left[\overline{(u'u')}^{\,n}_{k+1} - \overline{(u'u')}^{\,n+1}_{k}\right]_i - \frac{\phi^{n}_{k-\frac{1}{2}}}{\Delta z_k}\left[\overline{(u'u')}^{\,n-1}_{k} - \overline{(u'u')}^{\,n}_{k-1}\right]_i \Bigg\} - F\,\overline{u'u'}^{\,n+1} + R^n
$$

where R^n represents the advection and all other terms evaluated at time level n.

The Poisson equation is formed from the finite-difference equations by performing the divergence operation on them in finite-difference form (Williams, 1969). The divergence is forced to zero within round off error by adjusting the pressure through the inclusion of the divergence in the source term at time level $n-1$.

The Poisson equation is solved by an ADI iterative approach as,

$$
\left(r_\ell - \frac{\partial^2}{\partial x^2}\right)\bar{P}^{\bar{\ell}}_{i,k} = \left(r_\ell + \frac{\partial^2}{\partial z^2}\right)\bar{P}^{\ell}_{i,k} - S_{i,k}
$$

$$
\left(r_\ell - \frac{\partial^2}{\partial z^2}\right)\bar{P}^{\ell+1}_{i,k} = \left(r_\ell + \frac{\partial^2}{\partial x^2}\right)\bar{P}^{\bar{\ell}}_{i,k} - S_{i,k}
$$

where r_ℓ are the iteration parameters with ℓ denoting the iteration numbers. $P_{i,k}$ is the pressure and $S_{i,k}$ the source term on the grid point (i,k). The continuum second derivative operators are understood to represent their appropriate finite-difference analogues. The boundary conditions on the pressure are of the Neuman type, $\frac{\partial P}{\partial S} = G$, where s is the distance normal to the boundary and G is obtained by applying the mean field equations on the boundary. The optimum iteration parameters are calculated by the method outlined in Wachpress (1966). This method minimizes the maximum eigenvalue of the iteration matrix. The truncation error of the overall finite-difference scheme is between first and second order in time and space.

The restrictions on the time step are derived empirically by trying different time steps for a given problem of a given turbulent strength and Brunt-Vaissala frequency. The restriction on the time step for some types of terms as the non-linear transport terms, which are subject to the Courant-Friedericks-Lewy condition of $\Delta t \lesssim \Delta s/v_o$ where Δs is the smallest grid spacing and v_o is the largest velocity, is known. Similar insight can be

gained into the stability requirements due to some types of coupling between the equations that govern internal gravity waves, but even a partial linearized analysis of the equations becomes rapidly too time consuming. The non-physical computational mode that arises from the finite-differencing of the non-linear terms where a first order equation in time is raised to a second-order difference equation is eliminated by periodic averaging of the variables.

The boundary conditions on the mean field velocities are that the normal velocity vanishes and the normal derivative of the tangential velocity vanishes. For the Reynold and thermal stresses, we use the boundary condition of vanishing derivatives,

$$\frac{\partial}{\partial x_k} \overline{u_i' u_j'} = \frac{\partial}{\partial x_k} \overline{u_i' \rho'} = 0 .$$

REFERENCES

Bryan, K., "Monthly Weather Review" 94, 39, 1966.

Irwin, H. P. A. H., "Measurements in Boundary Layers and Their Prediction by Reynolds Stress Modelling", Ph. D. Thesis, McGuill University, Department of Mechanical Engineering, 1974.

Launder, B. E., "Turbulence Models and Their Experimental Verification", Penn. State lectures, 1974.

Launder, B. E., J. of Fluid Mech., 67, 569, 1975.

Lewellen, W. S., A. R. A. P. Report No. 226, 1974.

Piacsek, S. A., & Williams, G. P., J. of Computational Physics., 6, 392, 1970.

Roberts, G., Private Communication, 1972.

Warn-Varnas, A. C., Piacsek, S. A. and Dugan, J. P., Computers and Fluids 4, p. 109, 1976.

Wachspress, E. L. Iterative Solutions of Elliptic Systems, Prentice Hall 1966.

Williams, G. P., J. of Fluid Mech. 37, 727, 1969.

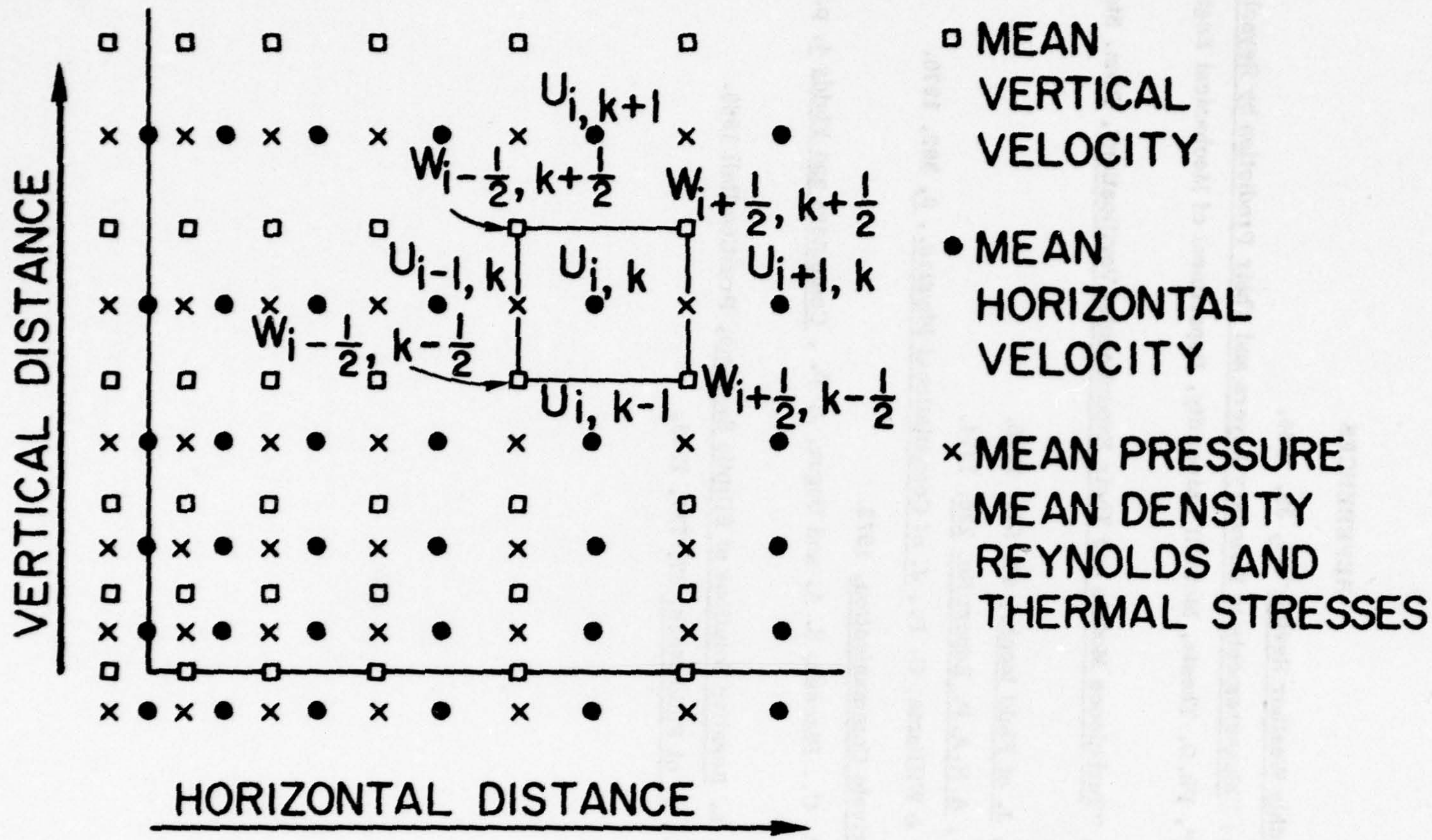

Fig. 1 - Staggered grid arrangement on which various mean and turbulence quantities are computed

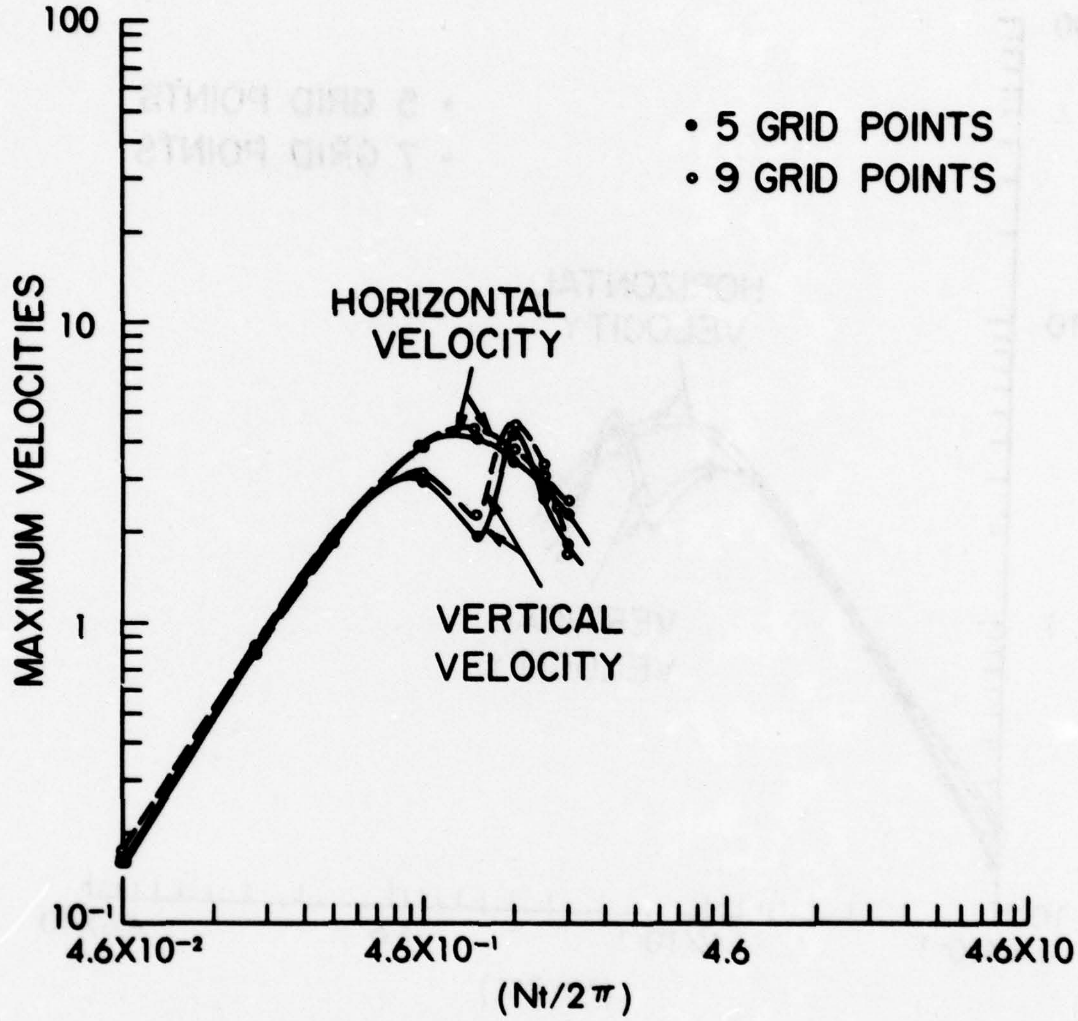

Fig. 2 - Comparison of maximum mean horizontal and vertical velocities obtained with different wake resolutions. Case a) places a constant grid of 5 points in the wake, and case b) a stretched grid of 9 points. The radius in each case is 15 cm and the total computed region is 100 cm x 100 cm.

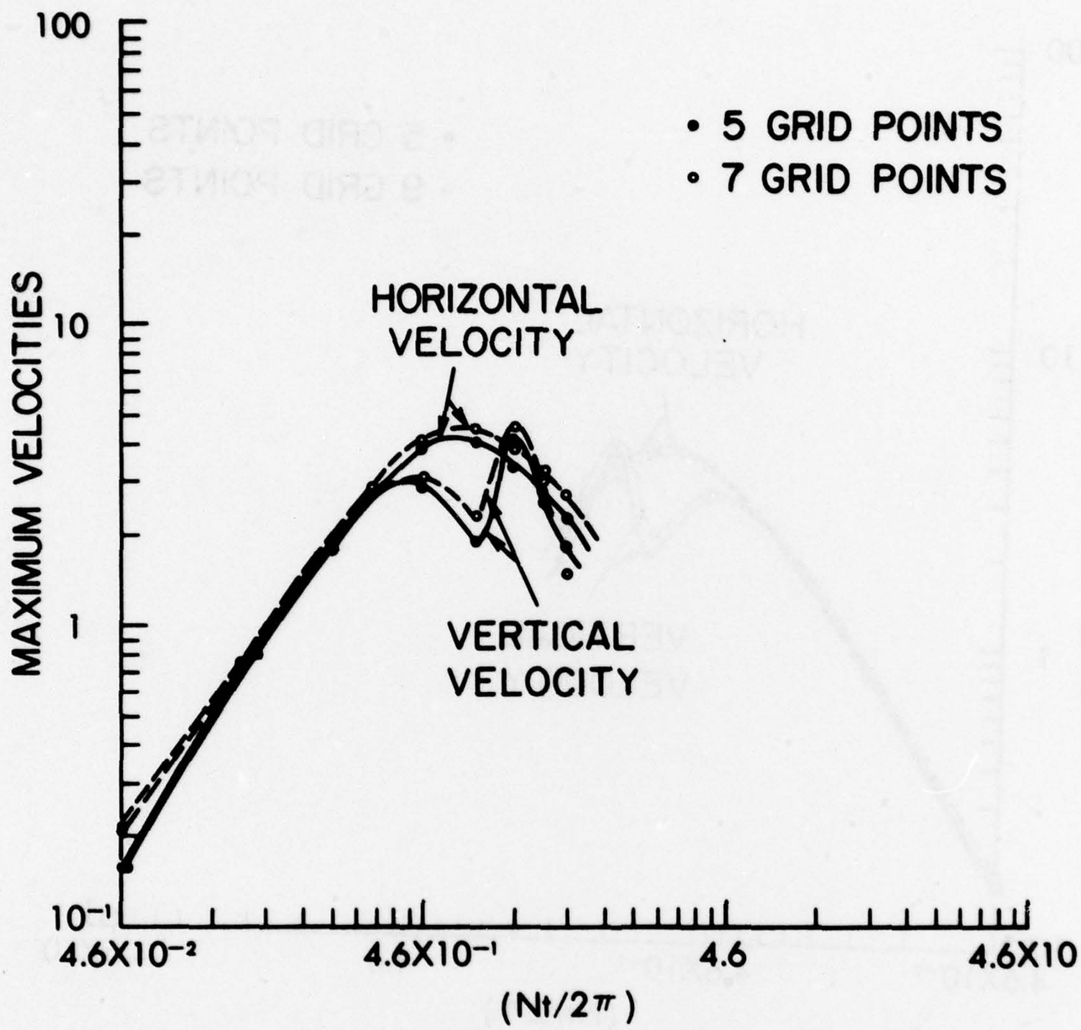

Fig. 3 - Continuation of Figure 2, with case a) again placing a constant grid of 5 points in the wake and case b) 7 points on a stretched grid. Here case b) had a total region size of 200 cm x 200 cm.

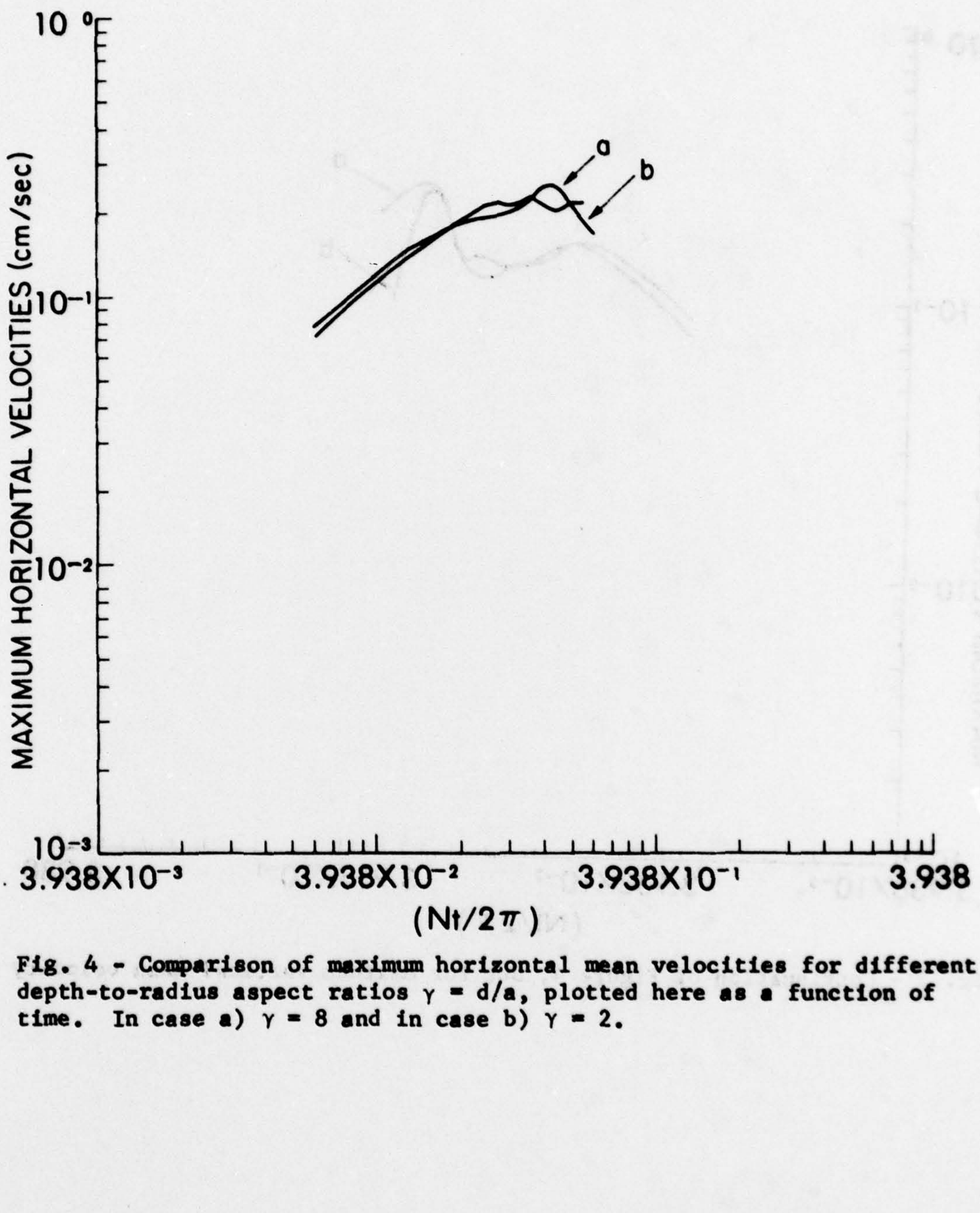

Fig. 4 - Comparison of maximum horizontal mean velocities for different depth-to-radius aspect ratios $\gamma = d/a$, plotted here as a function of time. In case a) $\gamma = 8$ and in case b) $\gamma = 2$.

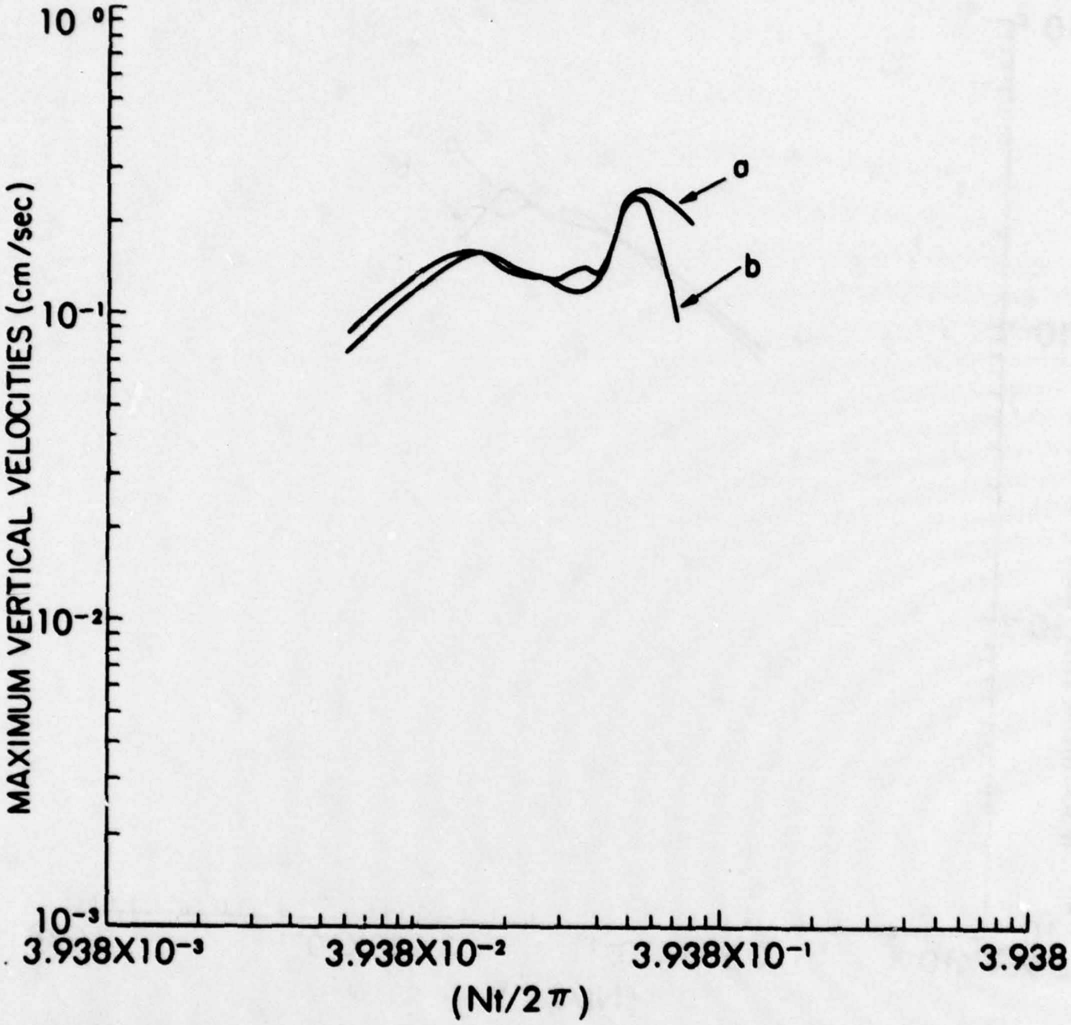

Fig. 5 - Continuation of Figure 4, but for maximum vertical mean velocity

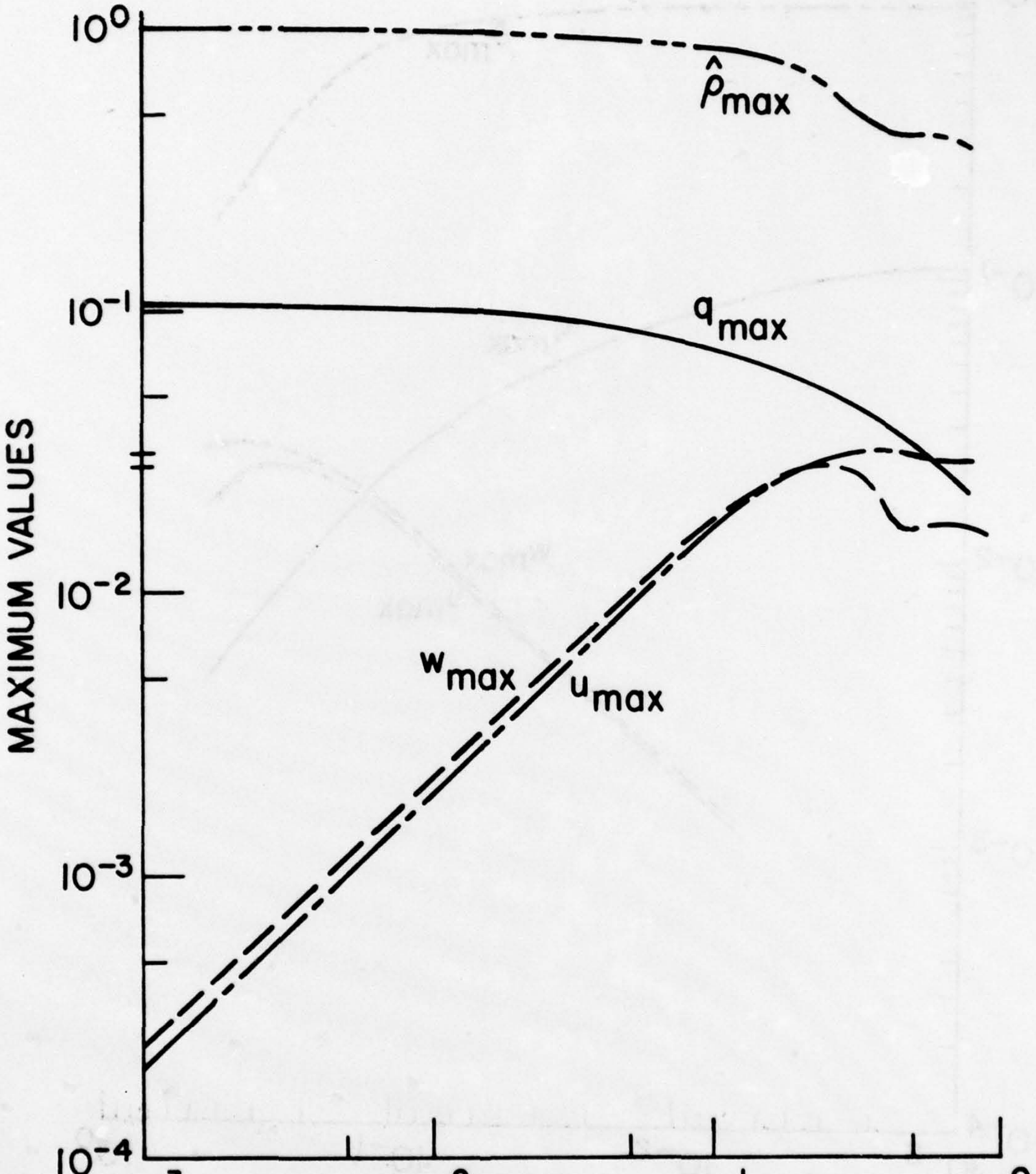

Fig. 6 - Plots of maximum mean horizontal and vertical velocity, maximum turbulent energy, and maximum mean density vs. time, as obtained by Lewellen (1974) for the LT case

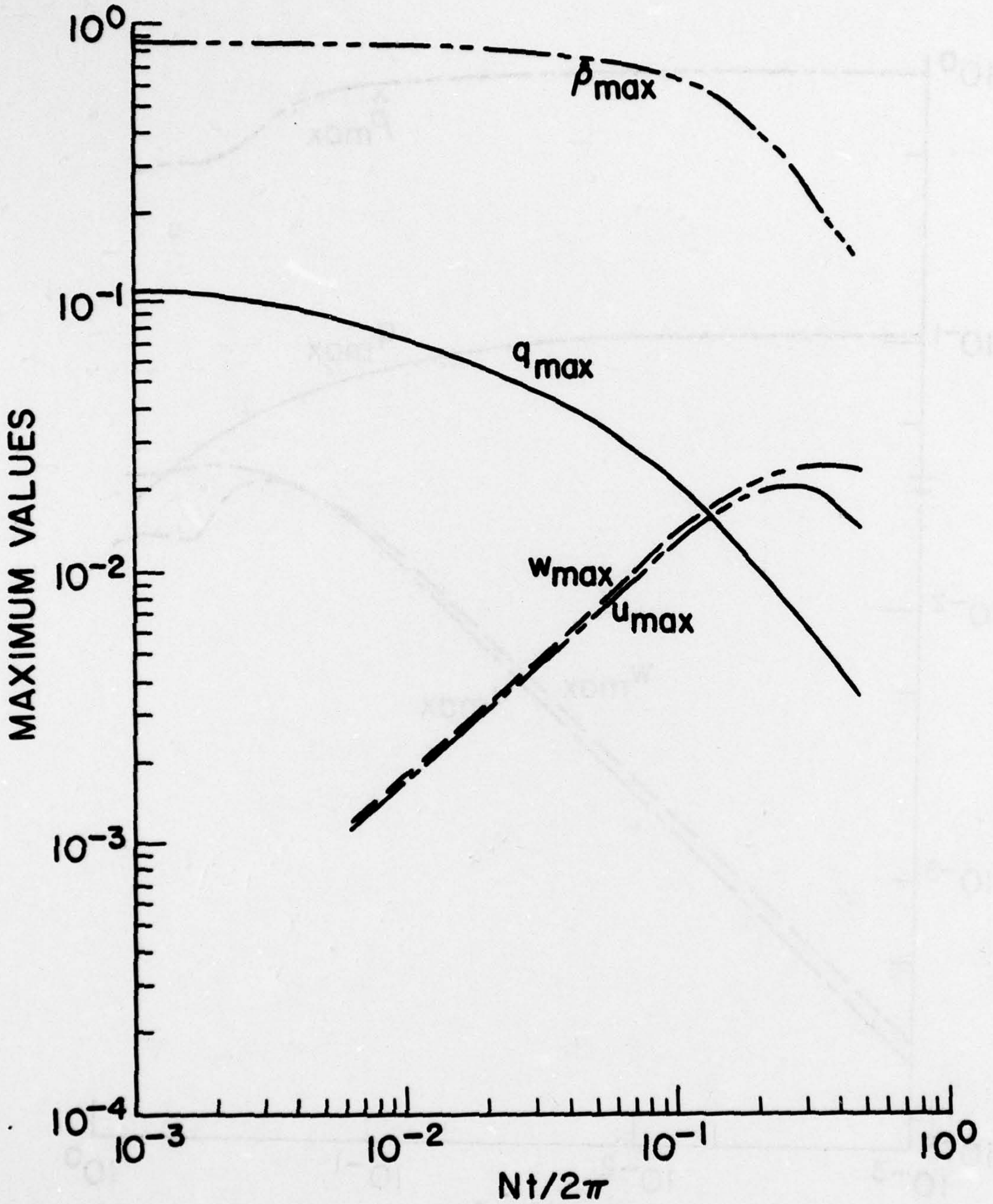

Fig. 7 - Same as Figure 6, but using the authors' first-order closure of turbulence, closure constants and numerical schemes

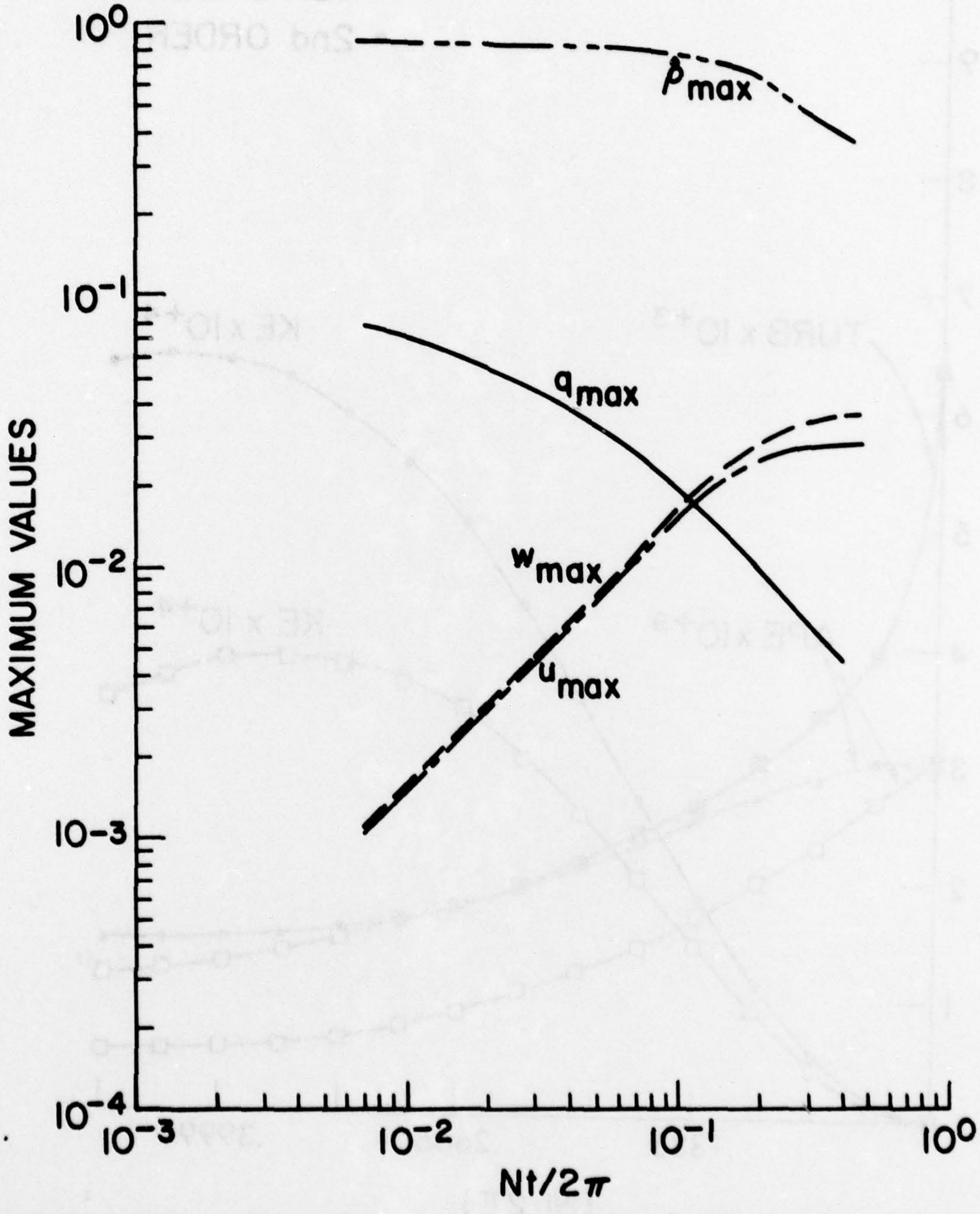

Fig. 8 - Same as Figure 7, but using the authors' second-order closure approximations, constants and numerics

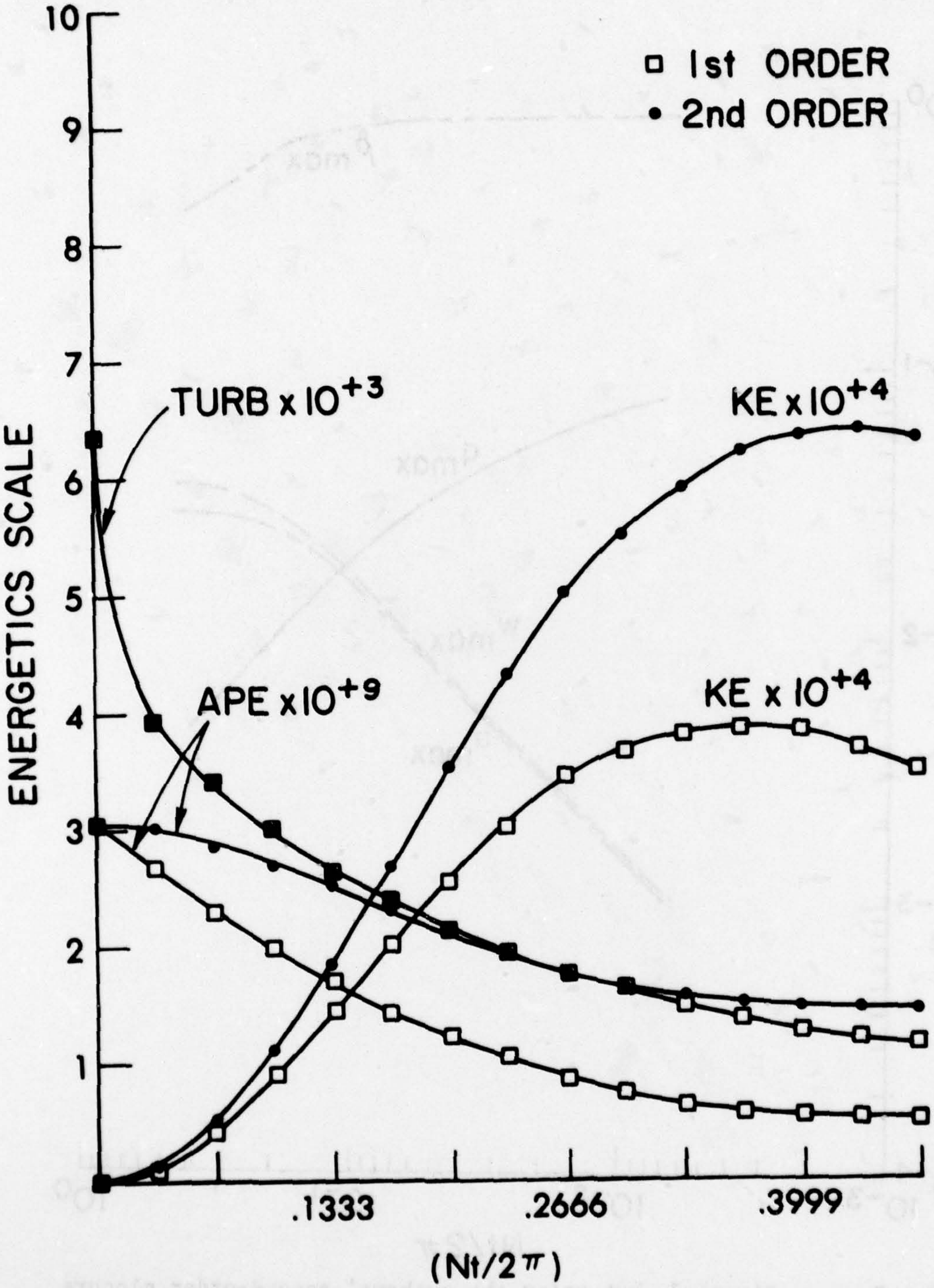

Fig. 9 - Comparison of the time evolution of available potential energy (APE), kinetic energy (KE) and turbulence energy (TURB) for 1st and 2nd order turbulence closure schemes

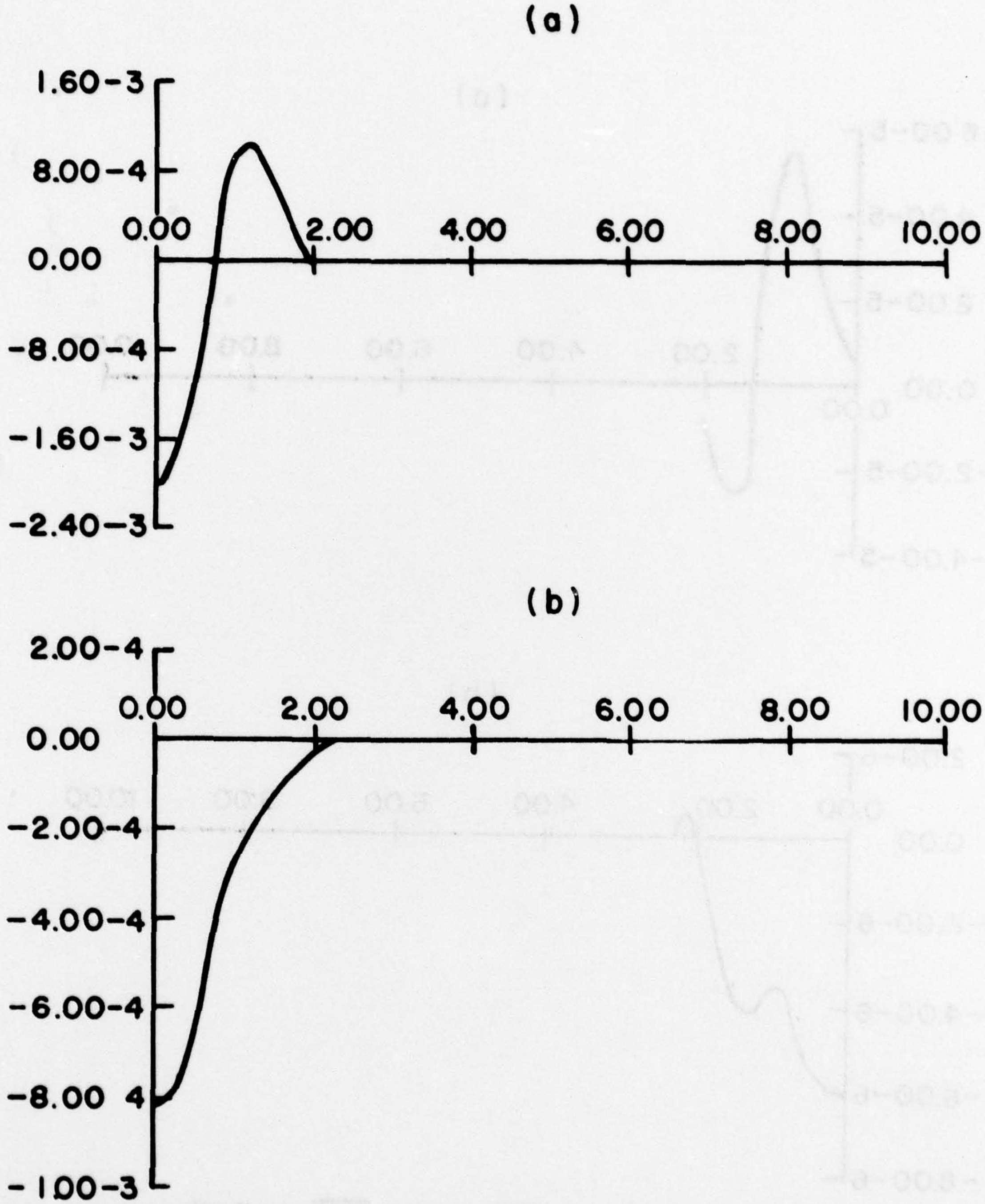

Fig. 10 - Plot of the thermal stress $\overline{w'\rho'}$ vs. depth at a horizontal distance of x/a = .57. Curve <u>a</u> represents 1st order closure and curve <u>b</u> 2nd order closure.

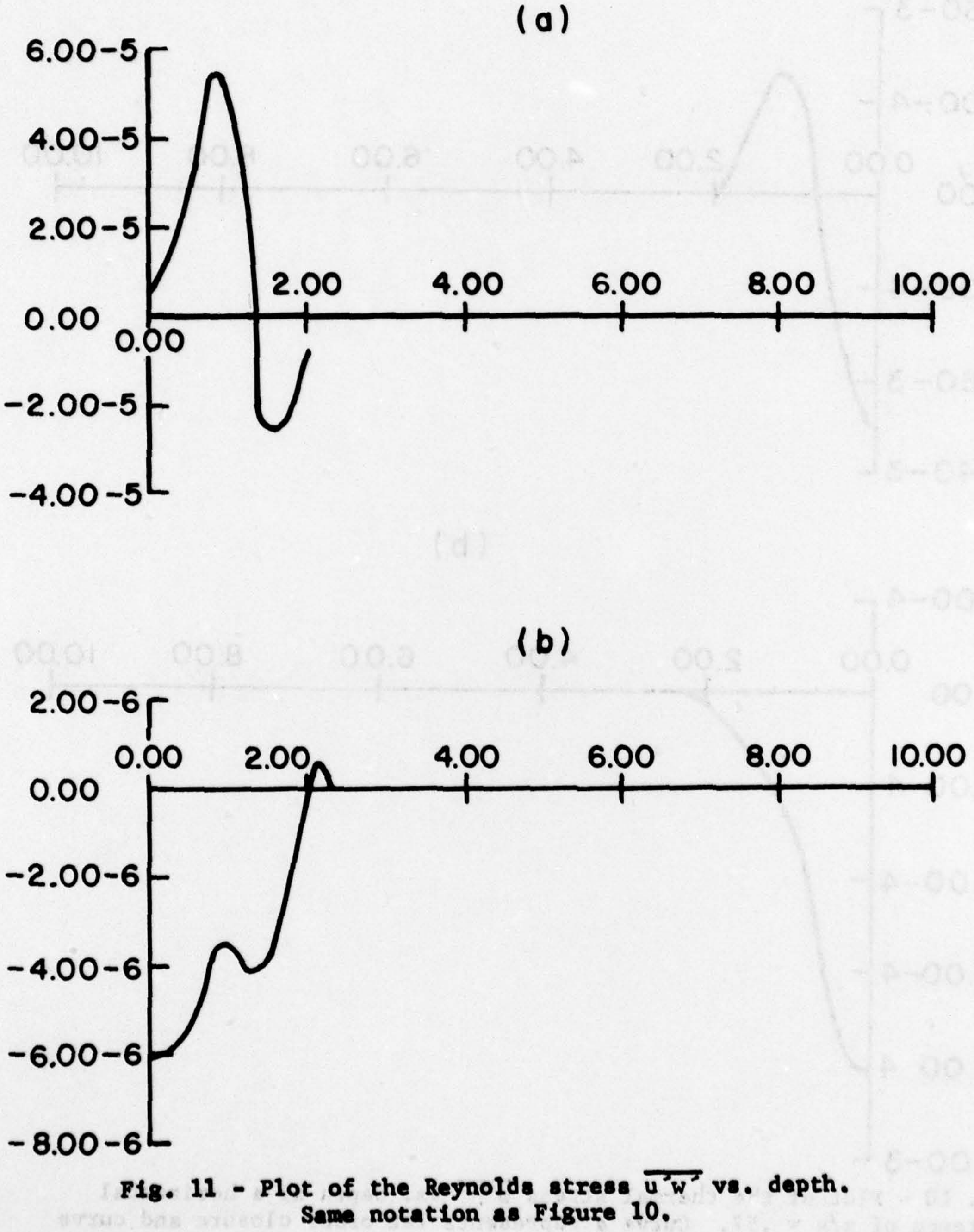

Fig. 11 - Plot of the Reynolds stress $\overline{u'w'}$ vs. depth.
Same notation as Figure 10.

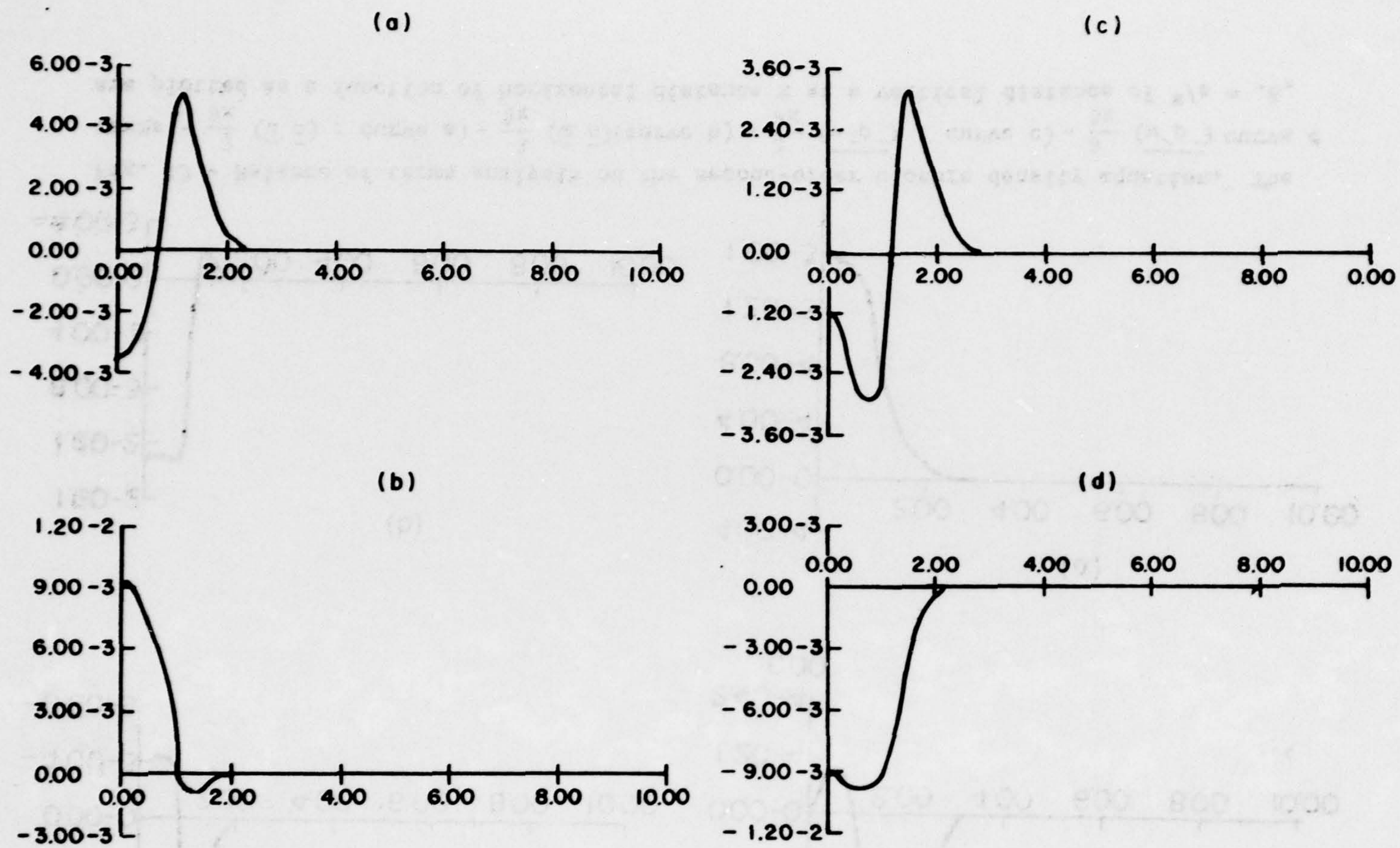

Fig. 12 - Balance of terms analysis on the first-order closure density equation. The terms $-\frac{\partial}{\partial x}(\bar{u}\,\bar{\rho})$: curve a) $-\frac{\partial}{\partial z}(\bar{w}\,\bar{\rho})$: curve b) $-\frac{\partial}{\partial x}(\overline{u'\rho'})$: curve c) $-\frac{\partial}{\partial z}(\overline{w'\rho'})$ curve d are plotted as a function of horizontal distance x at a vertical distance of $z/a = .6$.

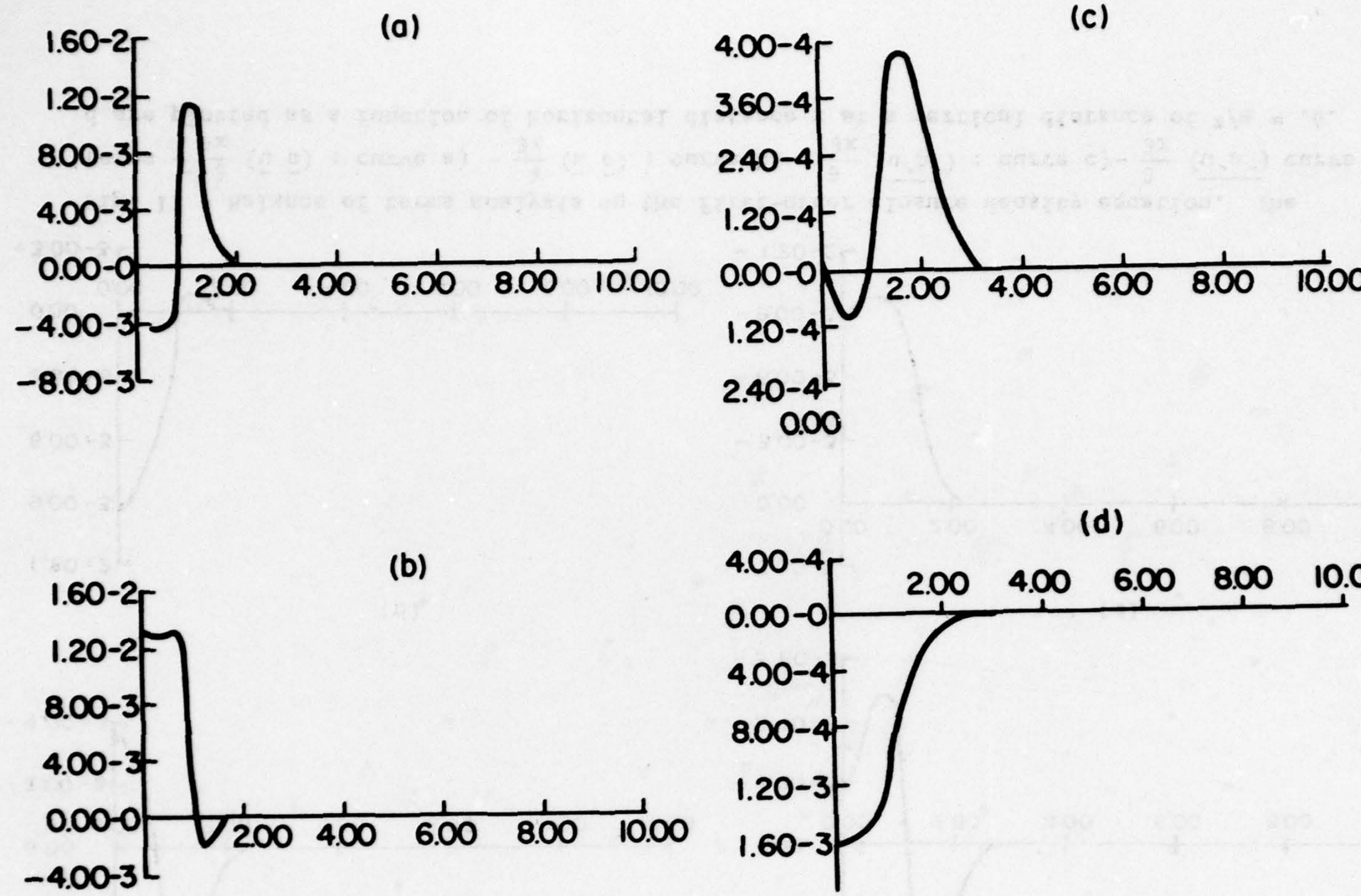

Fig. 13 - Balance of terms analysis on the second-order closure density equation. The terms $-\frac{\partial}{\partial x}(\bar{u}\,\bar{\rho})$: curve a) $-\frac{\partial}{\partial z}(\bar{w}\,\bar{\rho})$:curve b) $-\frac{\partial}{\partial x}\overline{(u'\rho')}$: curve c) $-\frac{\partial}{\partial z}\overline{(w'\rho')}$ curve d are plotted as a function of horizontal distance x at a vertical distance of $^{z}/a$ = .6.

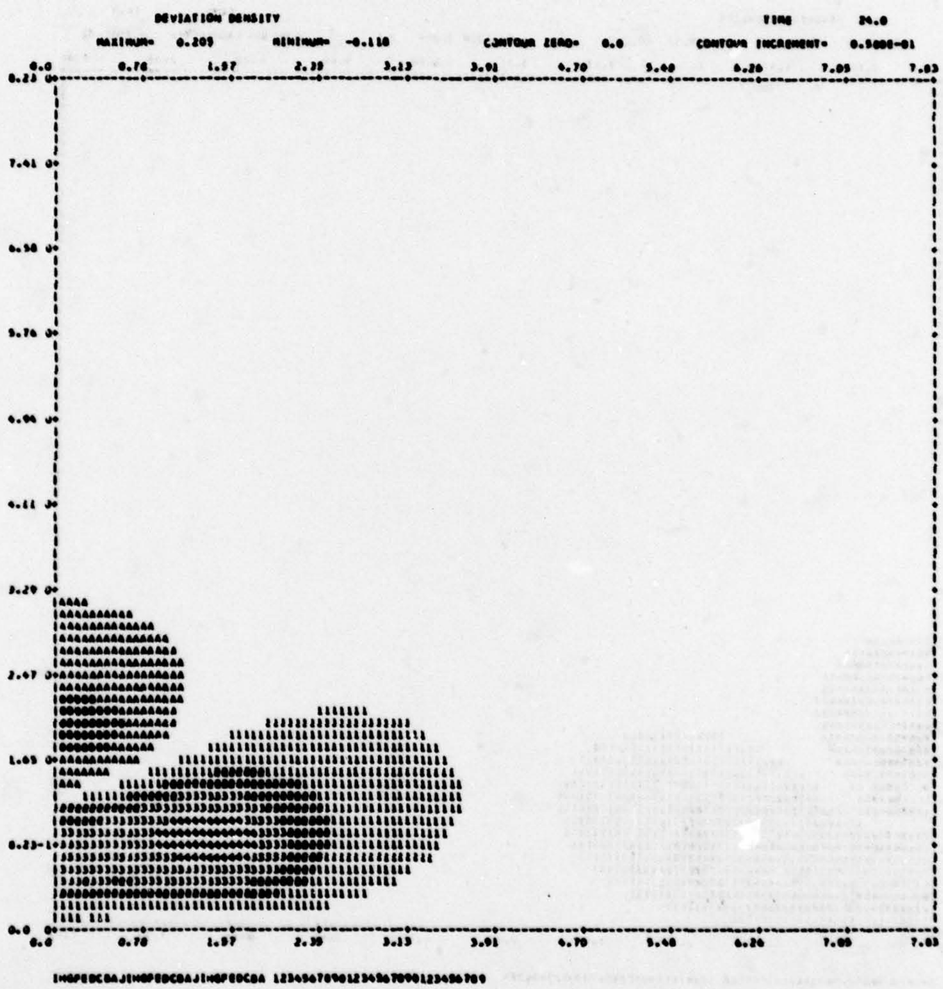

Fig. 14 - Contours of mean density (deviation from horizontal average) for the LT case, obtained with first-order closure

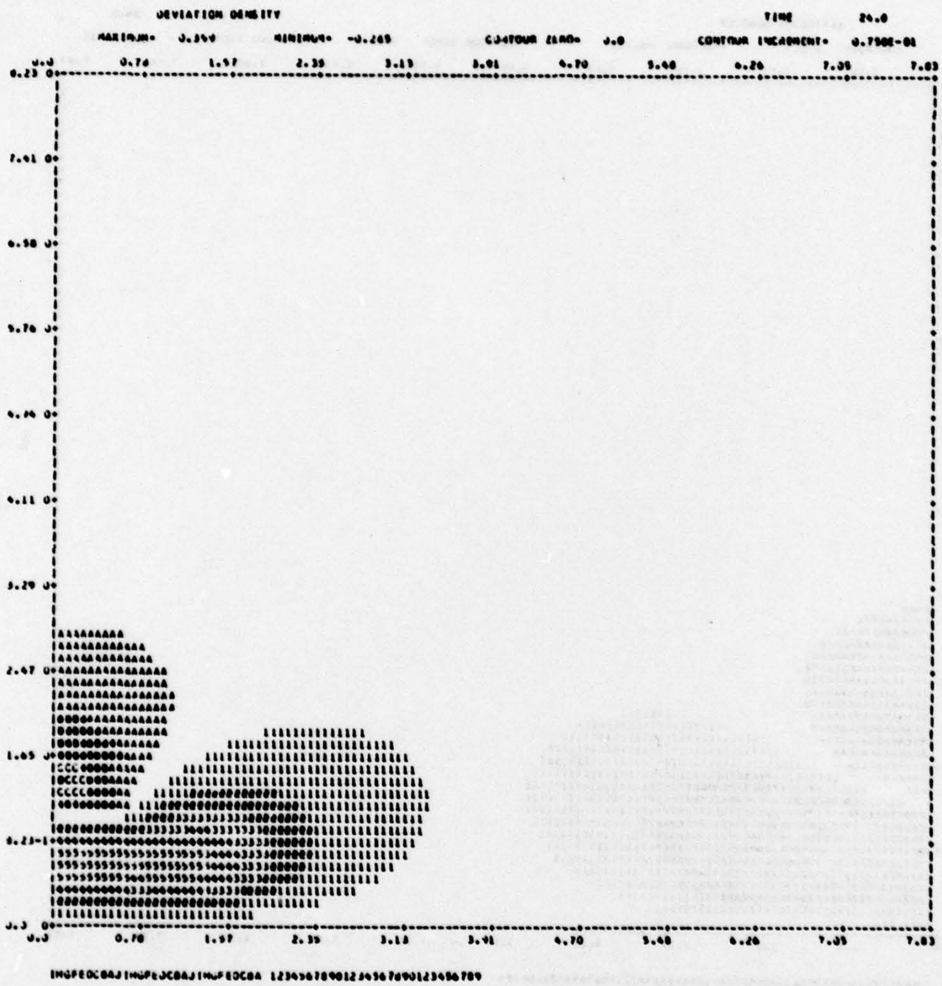

Fig. 15 - Contours of mean density (deviation from horizontal average) for the LT case, obtained with second-order closure

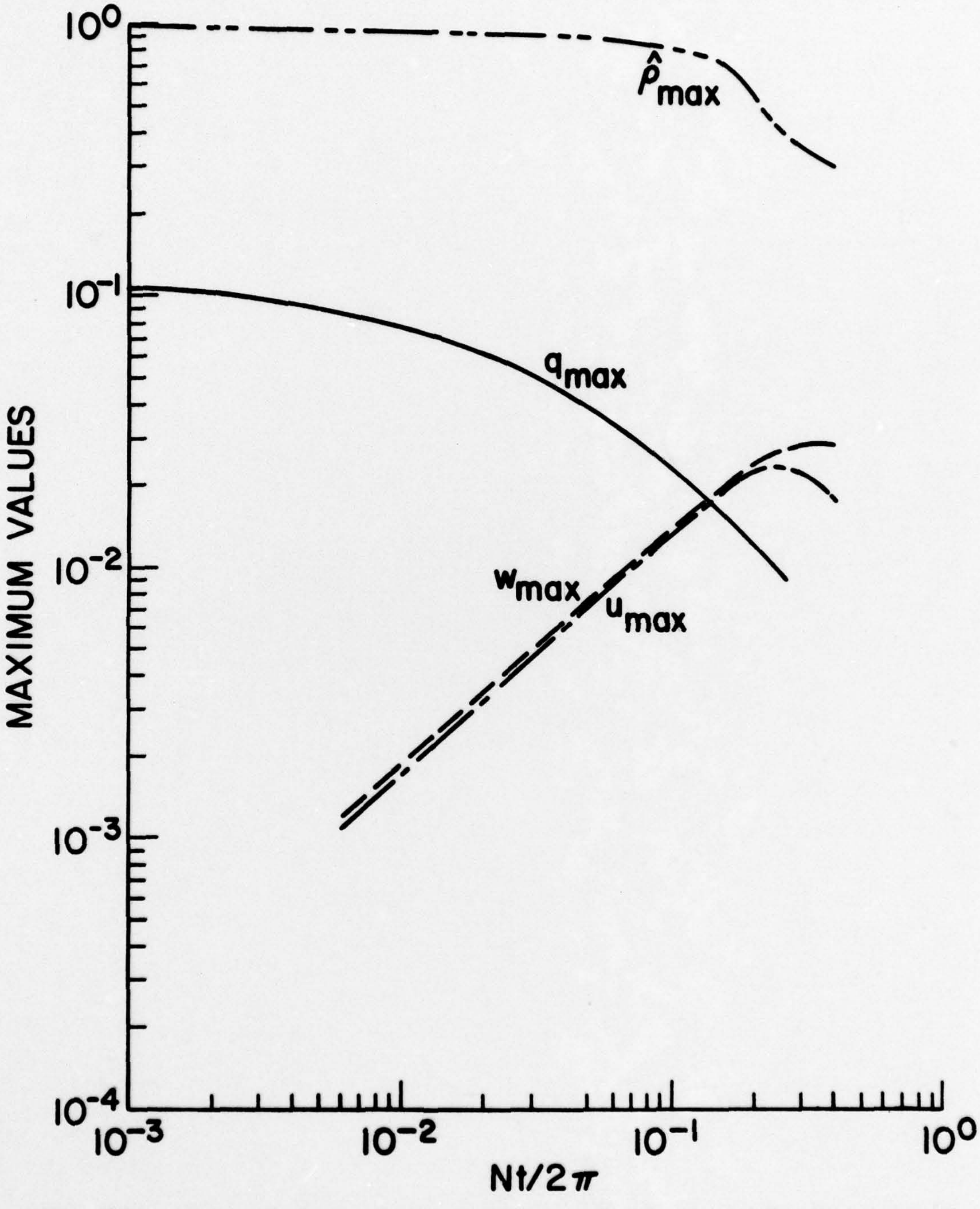

Fig. 16 - Plots of maximum mean density, mean horizontal and vertical velocity and turbulent energy vs. time for the LT case, but with the authors' closures and constants set to agree with Lewellen (1974)